Numerical simulations of glacial-valley longitudinal profile evolution

K.R. MacGregor
R.S. Anderson
S.P. Anderson
Department of Earth Sciences and Center for the Study of Imaging and Dynamics of the Earth, University of California, Santa Cruz, California 95064, USA
E.D. Waddington Geophysics Program, University of Washington, Seattle, Washington 98195, USA

ABSTRACT

Glaciers shape alpine landscapes. They broaden valley bottoms, enhance local valley relief, generate multiple steps, overdeepen valley floors, and cause tributary valleys to hang. These distinctive glacial signatures result from 10^4–10^5 yr of erosion, during which swings in climate drive advances and retreats of alpine glaciers. We use a numerical model of glacial erosion to explore the development of the longitudinal profiles of glaciated valleys. The model is driven by the past 400 k.y. of variable climate. Because both sliding speed, which dictates abrasion rate, and water-pressure fluctuations, which strongly modulate quarrying rate, should peak at the equilibrium-line altitude (ELA), we expect the locus of most rapid erosion to follow the transient ELA. Simulations of a single glacial valley show rapid flattening of the longitudinal profile. Inclusion of a tributary glacier creates a step immediately downvalley of the tributary junction that persists over multiple glaciations and commonly leaves the tributary valley hanging. Steps and overdeepenings result from an increase in ice discharge immediately below the tributary junction, which is accommodated primarily by increased ice thickness and hence sliding rate. The size of the step increases with the ratio of tributary to trunk ice discharge, while the height of a hanging valley reflects the difference in the time-integrated ice discharge in tributary and trunk valleys and therefore increases as the discharge ratio decreases.

Keywords: glacial erosion, hanging valley, longitudinal profile, landscape evolution, relief.

INTRODUCTION

Glaciated valleys are easily identified by U-shaped cross sections and characteristics of their longitudinal profiles that contrast strongly with fluvial valley forms. Although longitudinal profiles of rivers are typically smooth and decrease in slope downvalley, glaciated valleys have wide, low-gradient floors punctuated by multiple steps and overdeepenings tens to hundreds of meters deep (Fig. 1). Upon deglaciation, these bedrock-floored basins are evident as string-of-pearl lakes or sediment-filled meadows. Whereas fluvial tributaries join master streams at grade, glacial tributary valley floors are commonly tens to hundreds of meters above the trunk-valley floor. Despite this sharp contrast in valley forms and in erosion rates (Hallet et al., 1996), landscape evolution models have focused on river-dominated landscapes. Yet understanding the spatial and temporal patterns of bedrock removal by glaciers is a prerequisite for constraining valley-scale relief production and mountain-growth dynamics in high-altitude ranges.

Although the evolution of the glacial-valley cross section has been addressed (Harbor, 1992; Harbor et al., 1988), the development of longitudinal features in glacial valleys has received little attention. Oerlemans (1984) demonstrated that overdeepenings developed under deteriorating temperature histories. Alley et al. (1999) focused on overdeepenings that result from complex thermal and hydrologic conditions. Here we describe a numerical model designed to simulate evolution of the entire glacial longitudinal profile, including steps, overdeepenings, and hanging valleys. Valley profiles develop under the nonsteady climatic conditions that drive large changes in glacier thickness and length. Time scales derived from scaling of average subglacial erosion rates (1 mm/yr) and typical step and overdeepening relief (100 m), and similar time scales predicted for U-shaped valley formation (Harbor, 1992), suggest that such simulations must be run for at least 10^5 model yr.

One hypothesis for the generation of glaciated valley profiles is that steps or overdeepenings result from variations in glacier length over multiple climate cycles. Another is that high basal water pressure in existing overdeepenings (Alley et al., 1999; Hooke, 1991) can localize subglacial erosion. The ice-flow field, in some cases associated with tributary junctions, may be responsible for enhanced local erosion (Gutenberg et al., 1956; Nye and Martin, 1967). Some glacial geologists attribute gross valley morphology to nonuniform erodability, through variations in lithology, rock hardness, or joint spacing (Augustinus, 1995; Glasser et al., 1998), or in preglacial and/or proglacial mechanical and chemical weathering (Glasser and Hall, 1997; Lliboutry, 1994). Here we test the importance of glacial history and tributaries in setting the pattern of erosion. We choose a conservative rule set in which feedbacks that may enhance or focus erosion are minimized. Although proglacial fluvial processes play an important role in glacial valley geomorphology, we ignore this and focus on subglacial landform development.

NUMERICAL MODEL

We employ a one-dimensional, finite-difference staggered-grid model of a temperate valley glacier (Fig. 2; Table 1). Our treatment of the mass balance, ice motion, and ice discharge (Q_x) closely resembles other numerical models of ice flow (e.g., Bindschadler, 1982; Oerlemans, 1984, 1997; Waddington and Clarke, 1988). Local glacier mass balance (b) is calculated as the difference between precipitation and local melt (Fig. 2A). Precipitation increases linearly with initial valley elevation to a maximum; it is held steady for the duration of the simulation (Oerlemans, 1984). Melt is calculated as a function of air temperature with a positive degree-day approach (Braithwaite, 1995). Air temperature is tied to ice-surface elevation and varies sinusoidally over each model year. Cross-sectionally averaged ice velocity is the sum of local average internal deformation ($\overline{U}_d$) and basal sliding (U_s) velocities. Ice-deformation calculations assume Glen's flow law, and our basal sliding rule follows from Paterson (1994, p. 151, 252) (Table 1). To calculate the pattern of effective stress at the bed (N_e), we impose a water level that is everywhere 75 m less than local ice thickness (Oerlemans, 1984). Local basal shear stress (τ_b) is modified both by expo-

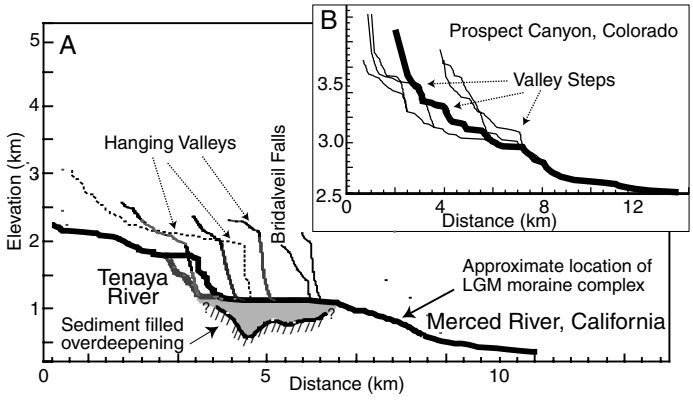

Figure 1. A: In Yosemite Valley, 600 m sediment-filled overdeepening occurs downstream of confluence of Tenaya and Merced Rivers (Gutenberg et al., 1956). Smaller tributaries hang above trunk stream. B: Prospect Canyon has stepped profile and contains numerous lakes. Tributaries hang above trunk, some joining trunk near lakes. LGM—last glacial maximum.

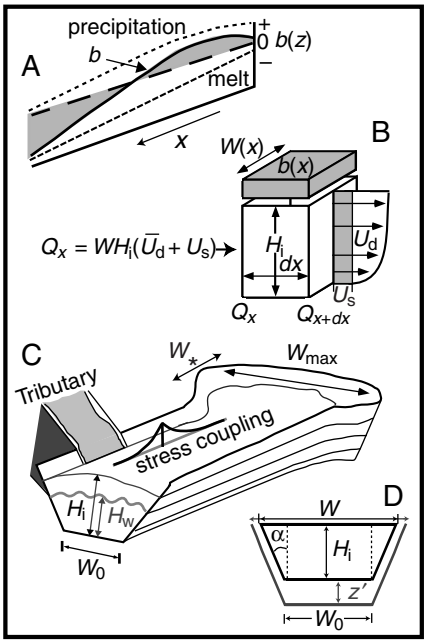

Figure 2. A: Mass balance is sum of local precipitation and melt and is zero at equilibrium line altitude B: Schematic of numerical model cell in which local mass balance acts at top, and ice discharge (*Q*) is calculated across cell edges. C: Width function, with widened accumulation area. D: Valley cross section is defined by valley bottom width (W_0) and trapezoid angle (α). See text for additional detail.

nential longitudinal stress coupling, the length scale of which is the local ice thickness (H_i) (Echelmeyer and Kamb, 1986; Kamb and Echelmeyer, 1986), and by a cross-sectional shape factor (F_1) (Paterson, 1994, p. 269). We prescribe a trapezoidal valley cross section (Oerlemans, 1997) with a spatially varying valley width $W(x)$ (Fig. 2C and 2D). Node spacing (dx) is typically 250 m over a valley sufficiently long (50 km) to display the full range of morphologic features. A tributary glacier is incorporated in most simulations. While the tributary glacier has its own initial elevation and width profiles, its treatment is identical to that of the trunk glacier. Ice from the tributary is added to the trunk glacier at the confluence.

Climatic variability is simulated by modulating the mean annual temperature at a reference elevation, Z_0, by a maximum of 6 °C, commensurate with a 1 km variation in equilibrium-line altitude (ELA) (Porter, 1989). The timing and amplitude of climate variation is set by oscillations in the marine $\delta^{18}O$ curve (Imbrie et al., 1984). All simulations were conducted using the most recent 400 k.y. of the $\delta^{18}O$ record.

TABLE 1. MODEL EQUATIONS AND PARAMETERS

Model	Equation or value
Glen's flow law (deformation rate of ice)	$\frac{du}{dz} = \frac{A}{2} \times \tau_{xz}^3$
Basal sliding rule	$U_s = \frac{C_1 \times \tau_b^2}{N_e}$
Basal shear stress	$\tau_b = F_1 \rho_i g H_i \sin(\theta)$
Effective stress	$N_e = \rho_i g H_i - \rho_w g H_w$
Ice deformation velocity	$\bar{U}_d = \frac{2A}{5} H_i \tau_b^3$
Glacier water table	$H_w = H_i - 75$ m
Shape factor	$F_1 = \frac{W}{(2 \times H_i)}$
Erosion rule	$\mathcal{E} = C_2 \times U_s$
Gravitational acceleration (g)	9.81 m•s^{-2}
Arrhenius constant (A)	2.1 x 10^{-16} Pa^{-3}•yr^{-1}
Trapezoid angle (α)	30°
Positive degree-day factor	0.006
Lapse rate	6 °C•km^{-1}
Reference elevation (Z_0)	1480 m
Reference temperature (T_0)	-1.5 °C
Yearly temperature amplitude	20 °C
Reference precipitation (P_0)	1.2 m
Precipitation gradient	1.3 m•km^{-1}
Precipitation maximum	2.2 m
Width minimum (W_0)	500 m
W_*, W_{max}	1000 m, 1200 m
ρ_i, ρ_w	917 kg•m^{-3}, 1000 kg•m^{-3}
Sliding coefficient (C_1)	0.0012 m•Pa^{-1}•yr^{-1}
Erosion coefficient (C_2)	0.0001

EROSION RULE

Abrasion, quarrying, chemical dissolution, and fluvial erosion all operate beneath temperate glaciers. We assume that the local erosion rate is proportional to the local basal sliding rate, which is important in both abrasion and quarrying (Hallet, 1979, 1996). Field measurements define the proportionality constant (Humphrey and Raymond, 1994). This rule does not explicitly incorporate subglacial water-pressure variability, which is critical in driving quarrying (Hallet, 1996). However, our rule produces a pattern of erosion similar to that expected from quarrying, i.e., one that reflects the annually integrated water-pressure field. Water flux increases downglacier, but water-pressure fluctuations likely follow a different pattern, dictated by the hydraulics of subglacial flow, bed geometry, and moulin distribution. Water pressures and their variations are high in "slow" cavity systems; "fast" conduits that relieve high water pressures develop progressively upvalley in the ablation zone each summer (Nienow et al., 1996, 1998). We therefore expect the annually averaged water-pressure field to display a maximum near the ELA, the upvalley extent of subglacial conduits (Nienow et al., 1998). Because the maximum in ice discharge and sliding rate also occurs near the ELA, a sliding-based erosion rule should mimic erosion associated with quarrying. Although there are no data on the spatial distribution of erosion at glacier beds, our erosion rule is physically plausible. Because we do not incorporate processes that create local zones of rapid erosion, such as focused water-pressure fluctuations at the headwalls of overdeepenings (Hooke, 1991) or hydraulic freeze-on (Alley et al., 1999), our erosion rule will produce bed profiles that are smoother than real glaciated valleys. Any steps or overdeepenings created in our simulations would be enhanced by these processes.

Our fixed-angle trapezoidal valley cross section is an important simplification in the model. Vertical lowering of the valley floor by z' results in valley widening of $2z'\tan(\alpha)$ (Fig. 2D). While the controls on glacial-valley widening are not well understood, constrictions of valley width may be important in creating overdeepenings (Merrand and Hallet, 1998). Although we do not specify valley-widening processes, we emphasize that our valley cross-section rule will not by itself focus erosion.

INITIAL MODEL CONDITIONS

We present four simulations, a control run without a tributary and runs with tributaries entering the trunk valley at 10, 20, and 30 km. Simulations are forced with the same climate (Fig. 3, inset) and begin under ice-free conditions. All initial valley profiles are slightly convex in the headwaters and feather to a constant downvalley slope, crudely simulating a fluvial profile in the upper reach. Tributaries are all 10 km long and a maximum of 1 km wide. They meet the trunk stream at grade, with a slope chosen such that the slope-area product of the tributary and the trunk valley are identical at the confluence. This condition of the initial fluvial system satisfies Playfair's law (Seidl and Dietrich, 1992).

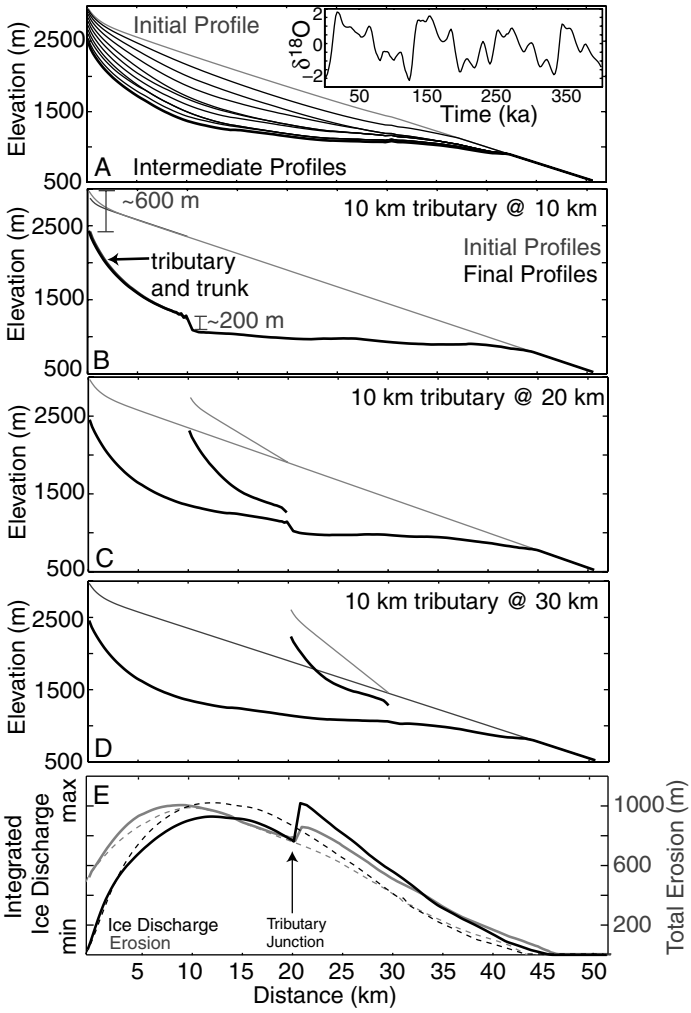

Figure 3. A: Control simulation with no tributary. Light gray line is initial valley profile; thin black lines are bed profiles at 40 k.y. intervals; thick black line is final profile after 400 k.y. Inset shows marine $\delta^{18}O$ curve over past 400 k.y. B: Tributary connecting to trunk valley at 10 km. Dark gray is initial tributary; light gray is initial trunk. Final profiles are the same, with 200 m step downvalley of confluence. C: Tributary at 20 km. Final trunk valley profile has sharp step with broad but slight overdeepening just downvalley. Tributary valley is hung by ~100 m. D: Tributary at 30 km. Only slight perturbation is evident in trunk valley, while tributary valley is hung by 200 m. E: Patterns of total erosion (gray) and long-term total ice discharge (black) in trunk valley. Simulations with no tributary (dashed lines) and with tributary connecting at 20 km (solid lines).

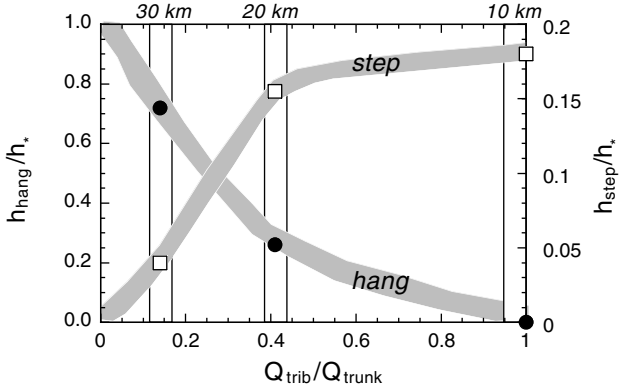

Figure 4. Heights of tributary valley hang (circles) and of trunk valley step (boxes) as functions of relative contribution of ice from tributary for each simulation (tributary location on top axis). *Q* is ice discharge. Hang and step heights are normalized by erosion of trunk valley immediately above confluence, h_*.

RESULTS

The modeled glacier fluctuations follow the driving temperature variations, with glacier termini reaching 40–45 km downvalley. A characteristic of all the final bed profiles is an increased concavity in the top 10 km of the valley and a flattened valley slope below. Thick ice (200–300 m) during full glacial periods and continuous occupation by smaller glaciers during interglacials erode the bed at the valley head (Fig. 3A). Subtle (10–25 m) overdeepenings are formed near each terminus stillstand. Overdeepenings formed early are smoothed and often erased by later advances. The final pattern of erosion in all simulations corresponds with the pattern of time-integrated ice discharge (Fig. 3E).

In runs with tributaries, the trunk and tributary glaciers advance and retreat past the tributary junction. An advancing tributary initially ponds against the trunk. Once a positive slope is established, tributary ice merges into the trunk glacier at a rate dictated by the tributary ice thickness and surface slope. For the tributary entering the trunk glacier at 10 km, the lengths and slopes of the two glacier branches above the junction are identical; a sharp, 200-m-high step in the valley develops below the confluence (Fig. 3B). The simulation with a tributary at 20 km develops hanging valley relief of ~100 m. In addition, a 100-m-high step forms in the main valley, immediately downstream of the junction, and a subtle 10-m-deep, 7-km-long overdeepening is generated, centered at 23 km (Fig. 3C). In contrast, the simulation with a tributary at 30 km produces a hanging valley with 200 m relief, but has little effect on the profile of the trunk valley (Fig. 3D).

DISCUSSION

The simulation with no tributary shows rapid steepening of the headwall and lowering of the slope elsewhere in the long profile. If the ridges above the valley undergo little erosion, significant valley-ridge relief will be generated. The valley profile is smooth, displaying neither significant nor persistent steps, even in the face of glacial advances of distinctly different length. Runs using an initially concave fluvial profile develop similar features with slightly reduced bed relief. At mean erosion rates of 1 mm/yr, a typical glacial advance will accomplish only ~20 m of erosion. Subtle steps and overdeepenings can easily be destroyed by subsequent glaciations of different length. Persistent multiple valley steps and overdeepenings therefore cannot be attributed to multiple glaciations with our sliding-based erosion rule.

The addition of a single tributary that undergoes the same altitudinally dependent climatic forcing decouples the trunk and tributary valley floors. The tributary valley is left hanging, and either a step or an overdeepening develops on the trunk valley floor immediately downvalley of the confluence. Both the reduction of the tributary surface slope due to ice ponding against the trunk glacier and the contrast between tributary and trunk ice discharge per unit width contribute to hanging the tributary. The rate of production of hanging valley relief increases strongly as the ratio of the tributary to trunk ice discharge decreases (Fig. 4).

Steps or overdeepenings in the trunk valley can be attributed to increased ice discharge below a tributary junction. This increase in discharge results in part from faster sliding, which in turn increases the local rate of erosion. The size of the step in the trunk valley increases as the ratio of the ice discharge in the tributary valley to that in the trunk valley increases (Fig. 4). Multiple tributaries could therefore explain multiple valley steps and overdeepenings.

In all simulations, the initially high bed- and ice-surface elevations access colder local temperatures that produce glaciers extending far downvalley. As erosion proceeds and the glacier bed lowers, the ice-surface elevation declines, promoting less positive mass balances for the same climatic pattern. This self-defeating mechanism was observed in simulations of

Oerlemans (1984), who required decreasing temperatures to develop overdeepenings. Such a feedback provides one explanation for the existence of older moraines downvalley of last glacial maximum complexes, despite the apparent strength of the last glacial maximum in the marine oxygen isotope record. Our calculations maximize this self-defeating effect because we have omitted (1) flexural isostatic compensation for erosion, (2) reduction of direct radiation to the valley floor by enhanced valley-ridge relief (Olyphant, 1986), and (3) reduced ablation owing to debris cover (Anderson, 2000; Clark et al., 1994; Lundstrom et al., 1993). All of these processes promote longer glaciers.

That cirques are conspicuously absent in the final profiles is likely related to our treatment of the headwall. We have not incorporated positive mass-balance feedbacks that might steepen headwalls, such as reduction of short-wave radiation and avalanching of snow onto the glacier. We intend to consider these positive feedbacks in future work.

CONCLUSIONS

Persistent, high-relief steps and overdeepenings in longitudinal profiles are generated in our simulations only when we incorporate tributary glaciers. The long-term erosion pattern in glaciated valleys mimics closely the long-term, integrated pattern of ice discharge. Our model profiles are smooth because processes that may be important in developing small-scale valley-floor roughness are not incorporated in our sliding-based erosion rule. Relief at tributary junctions and valley steps should vary in a predictable fashion in accord with the location and size of the tributary relative to the long-term ice-discharge maximum in the trunk valley. By extension, we suggest that the strong convergence of flow from ice-sheet interiors into narrow valleys at the ice-sheet margin may similarly promote the development of glacial fjords.

ACKNOWLEDGMENTS

This work was supported by National Science Foundation grants OPP98-18251 (University of California, Santa Cruz) and OPP98-19056 (University of Washington), and a NASA Graduate Fellowship (to MacGregor). We thank Kurt Cuffey for his insightful critique of the manuscript. Center for the Study of Imaging and Dynamics of the Earth contribution 421.

REFERENCES CITED

Alley, R.B., Strasser, J.C., Lawson, D.E., Evenson, E.B., and Larson, G.J., 1999, Some glaciological and geological implications of basal ice accretion in overdeepenings, *in* Mickelson, D.M., and Attig, J.W., eds., Glacial processes past and present: Geological Society of America Special Paper 337, p. 1–9.

Anderson, R.S., 2000, Evolution of medial moraines: Journal of Glaciology (in press).

Augustinus, P.C., 1995, Glacial valley cross-profile development: The influence of in situ rock stress and rock mass strength, with examples from the Southern Alps, New Zealand: Geomorphology, v. 14, p. 87–97.

Bindschadler, R., 1982, A numerical model of temperate glacier flow applied to the quiescent phase of a surge-type glacier: Journal of Glaciology, v. 28, p. 239–265.

Braithwaite, R.J., 1995, Positive degree-day factors for ablation on the Greenland ice sheet studied by energy-balance modelling: Journal of Glaciology, v. 41, p. 153–160.

Clark, D.H., Clark, M.M., and Gillespie, A.R., 1994, Debris-covered glaciers in the Sierra Nevada, California, and their implications for snowline reconstructions: Quaternary Research, v. 41, p. 139–153.

Echelmeyer, K.A., and Kamb, B., 1986, Stress-gradient coupling in glacier flow: II. Longitudinal averaging in the flow response to small perturbations in ice thickness and surface slope: Journal of Glaciology, v. 32, p. 285–298.

Glasser, N.F., and Hall, A.M., 1997, Calculating Quaternary glacial erosion rates in northeast Scotland: Geomorphology, v. 20, p. 29–48.

Glasser, N.F., Crawford, K.R., Hambrey, M.J., Bennett, M.R., and Huddart, D., 1998, Lithological and structural controls on the surface wear characteristics of glaciated metamorphic bedrock surfaces: Ossian Sarsfjellet, Svalbard: Journal of Geology, v. 106, p. 319–329.

Gutenberg, B., Buwalda, J.P., and Sharp, R.P., 1956, Seismic explorations on the floor of Yosemite Valley, California: Geological Society of America Bulletin, v. 67, p. 1051–1078.

Hallet, B., 1979, A theoretical model of glacial abrasion: Journal of Glaciology, v. 23, p. 39–50.

Hallet, B., 1996, Glacial quarrying: A simple theoretical model: Annals of Glaciology, v. 22, p. 1–8.

Hallet, B., Hunter, L., and Bogen, J., 1996, Rates of erosion and sediment evacuation by glaciers: A review of field data and their implications: Global and Planetary Change, v. 12, p. 213–235.

Harbor, J.M., 1992, Numerical modeling of the development of U-shaped valleys by glacial erosion: Geological Society of America Bulletin, v. 104, p. 1364–1375.

Harbor, J.M., Hallet, B., and Raymond, C.F., 1988, A numerical model of landform development by glacial erosion: Nature, v. 333, p. 347–349.

Hooke, R.L., 1991, Positive feedbacks associated with erosion of glacial cirques and overdeepenings: Geological Society of America Bulletin, v. 103, p. 1104–1108.

Humphrey, N.F., and Raymond, C.F., 1994, Hydrology, erosion and sediment production in a surging glacier; Variegated Glacier, Alaska, 1982–83: Journal of Glaciology, v. 40, p. 539–552.

Imbrie, J., Hays, J.D., Marinson, D.G., McIntyre, A., Mix, A., Morley, J.J., and Pisias, N.G., 1984, The orbital theory of Pleistocene climate: Support from a revised chronology of the marine $\delta^{18}O$ record, *in* Berger, A., et al., eds., Milankovitch and climate: Understanding the response to astronomical forcing, Volume 1: Higham, Massachusetts, D. Reidel, p. 269–305.

Kamb, B., and Echelmeyer, K.A., 1986, Stress-gradient coupling in glacier flow: I. Longitudinal averaging of the influence of ice thickness and surface slope: Journal of Glaciology, v. 32, p. 267–284.

Lliboutry, L., 1994, Monolithologic erosion of hard beds by temperate glaciers: Journal of Glaciology, v. 40, p. 433–450.

Lundstrom, S.C., McCafferty, A.E., and Coe, J.A., 1993, Photogrammetric analysis of 1984–89 surface altitude change of the partially debris-covered Eliot Glacier, Mount Hood, Oregon, U.S.A.: Annals of Glaciology, v. 17, p. 167–170.

Merrand, Y., and Hallet, B., 1998, Modeling the evolution of glaciated mountain ranges guided by field studies in the high coastal mountains of southern Alaska: Eos (Transactions, American Geophysical Union), v. 79, p. F337.

Nienow, P.W., Sharp, M., and Willis, I.C., 1996, Velocity-discharge relationships derived from dye tracer experiments in glacial meltwaters: Implications for subglacial flow conditions: Hydrological Processes, v. 10, p. 1411–1426.

Nienow, P., Sharp, M., and Willis, I., 1998, Seasonal changes in the morphology of the subglacial drainage system, Haut Glacier D'Arolla, Switzerland: Earth Surface Processes and Landforms, v. 23, p. 825–843.

Nye, J.F., and Martin, P.C.S., 1967, Glacial erosion, Volume 79: Bern, International Union of Geodesy and Geophysics, Commission on Snow and Ice, p. 78–86.

Oerlemans, J., 1984, Numerical experiments on large-scale glacial erosion: Zeitschrift für Gletscherkunde und Glazialgeologie, v. 20, p. 107–126.

Oerlemans, J., 1997, A flowline model for Nigardsbreen, Norway: Projection of future glacier length based on dynamic calibration with the historic record: Annals of Glaciology, v. 24, p. 382–389.

Olyphant, G.A., 1986, Longwave radiation in mountainous areas and its influence on the energy balance of alpine snowfields: Water Resources Research, v. 22, p. 62–66.

Paterson, W.S.B., 1994, The physics of glaciers: Tarrytown, New York, Pergamon and Elsevier Science, 480 p.

Porter, S.C., 1989, Some geological implications of average Quaternary glacial conditions: Quaternary Research, v. 32, p. 245–261.

Seidl, M.A., and Dietrich, W.E., 1992, The problem of channel erosion into bedrock: Catena supplement, v. 23, p. 101–124.

Waddington, E.D., and Clarke, G.K.C., 1988, Stable isotope pattern predicted in surge-type glaciers: Canadian Journal of Earth Sciences, v. 25, p. 657–668.

Manuscript received May 4, 2000
Revised manuscript received August 17, 2000
Manuscript accepted August 25, 2000